Meles, Mehari; Rajasekaran, Akash; Mela, Lauri; Jantti, Riku

# RIS-Assisted Three-Dimensional Drone Localization and Tracking Under Hardware Impairments

*Published in:*
IEEE Access

*DOI:*
10.1109/ACCESS.2024.3411309

Published: 01/01/2024

IEEE Access
Multidisciplinary | Rapid Review | Open Access Journal

Received 24 May 2024, accepted 3 June 2024, date of publication 7 June 2024, date of current version 17 June 2024.

*Digital Object Identifier 10.1109/ACCESS.2024.3411309*

RESEARCH ARTICLE

# RIS-Assisted Three-Dimensional Drone Localization and Tracking Under Hardware Impairments

**MEHARI MELES, (Member, IEEE), AKASH RAJASEKARAN, LAURI MELA, AND RIKU JÄNTTI, (Senior Member, IEEE)**

Department of Information and Communications Engineering, School of Electrical Engineering, Aalto University, 02150 Espoo, Finland

Corresponding author: Mehari Meles (mehari.meles@aalto.fi)

This work was supported by the Business Finland Project Drolo II.

**ABSTRACT** The concept of Reconfigurable Intelligent Surfaces (RIS) has emerged as a promising method for communications and the localization of aeronautical vehicles. In this paper, we explore the impact of hardware impairments on three-dimensional (3D) drone localization within a single-input single-output (SISO) system assisted by RIS. Our methodology begins by modeling the channel from the base station (BS), equipped with a single-antenna transmitter, to each RIS at known positions. This model accounts for hardware impairments at the BS, particularly beam downtilt, which influences the accuracy of drone location estimation. Moreover, we model the channel from the RIS to the drone, employing exhaustive beam sweeping in both azimuth and elevation angles to estimate the Angles of Departure (AODs) from the RIS to the drone. We adopt a unique phase noise (PN) model for each element within the RIS and assess the impact of these impairments on angle and location estimation accuracy through extensive simulations. Additionally, we examine the effects of RIS configuration and the Inter-Site Distance (ISD) between two RIS units on localization performance. An Unscented Kalman Filter (UKF) algorithm is integrated for tracking of the drone trajectory. Our simulation results demonstrate that the RIS-assisted 3D drone localization approach achieves significant accuracy despite various impairments. The findings of this paper underscore the potential of RIS-enabled 3D drone localization to maintain high accuracy under hardware impairments, paving the way for future research in RIS-enabled drone localization systems.

**INDEX TERMS** AOD, localization, RIS, UKF, drone.

## I. INTRODUCTION

Drones are increasingly essential for various applications, with accurate localization and tracking being critical to their operation. Traditional localization methods, like Global Positioning System (GPS), face challenges in urban environments due to non-line-of-sight (NLOS) cases. The use of radio frequency (RF) signals for drone localization has been extensively explored in literature [1], [2], [3], [4], [5]. Researchers are investigating Reconfigurable Intelligent Surface (RIS) methods as an alternative to base stations (BS) for drone localization. Recently, there has been an increasing trend in utilizing RIS in communication technologies due to their flexibility, cost-effectiveness, and energy efficiency. These surfaces enhance wireless communication performance by modifying signal propagation path in transmitters and receivers [6]. Specifically in radio localization, the deployment of Reconfigurable Intelligent Surfaces (RISs) creates additional reflected signal paths, providing new degrees of freedom to the localization model [7], [8]. The RIS primarily performs two operations: it aggregates and directs the energy from its elements [9], and it concentrates incoming electromagnetic waves towards the drone's location [10].

The associate editor coordinating the review of this manuscript and approving it for publication was Li He.

### A. RELATED WORKS

Research conducted in [11] and [12] shows that RIS-enabled technologies are considered one of the key enablers of localization, with further investigations into RIS-assisted localization presented in [13]. The study in [14] addresses the challenge of joint three-dimensional localization with its synchronization in a single-input single-output (SISO) system using a RIS. Simulation results demonstrate the capability of RIS-assisted wireless systems to provide accuracy of sub-meter in positioning, even with a single antenna both at the base station (BS) and the user equipment (UE). Furthermore, this study highlights the impact of the RIS element count on positioning accuracy.

Extensive research has developed in the field of RIS-aided localization, producing numerous publications [15], [16]. RISs offer significant benefits for solving complex localization issues, especially in single-antenna systems at the UE and BS, in both line-of-sight (LoS) and NLoS environments [14], [15]. The concept of applying a Large Intelligent Surface (LIS) to millimeter-wave (mmWave) positioning method is introduced in [16]. This body of work investigates the theoretical limits of positioning accuracy and examines the influence of LIS element count and phase shifter configurations on location estimation accuracy.

The paper [17] thoroughly explores bi-static sensing for positioning in single-input single-output systems, in which the position of both the transmitter and receiver are known locations. It derives the Cramer-Rao Bounds (CRBs) for estimation errors in both the position and orientation of RIS, and the time of arrival (TOA) in the transmitter-RIS-receiver path. Additionally, the paper proposes a multiple stage with low-complexity estimator employed for RIS localization, and it examines factors affecting location accuracy, including RIS size, system bandwidth, and the position of the RIS and orientation. In our preceding study [18], we detailed experiments on GPS-independent drone localization using two synchronized $4 \times 4$ rectangular antenna arrays. A single transmitting antenna was attached at the drone, and Multiple Signal Classification (MUSIC) algorithm was utilized to determine the Angle of Arrival (AOA) in the two arrays. Furthermore, an Extended Kalman Filter (EKF) was employed to continuously track the position of the drone over time.

The study in [19] presents a novel method for positioning estimation assisted by RIS in an asynchronous millimeter-wave SISO system. This method primarily focuses on designing the RIS phase and estimating channel parameters using the Inverse Fast Fourier Transform (IFFT) and the quasi-Newton method. It also involves positioning the user based on the spatial broadband effect of millimeter-wave technology. The research demonstrates through simulation that this localization method outperforms traditional narrow-band positioning techniques, especially at higher bandwidths, offering more significant improvements in accuracy. RISs possess the ability to enhance positioning accuracy.

The study in [19] explores a positioning system that comprises a BS and a RIS with known locations to estimate the positions of Mobile Stations (MSs). The research introduces an novel method Cooperative Positioning (CP) designed to address this challenge. Here, the RIS applies beam sweeping to search the main beams towards areas of interest. Each MS measures the strength of the signal received from these directed beams, thereby ascertaining its relative direction with respect to the RIS. The study presented in [20] explores the utilization of RIS to demonstrate the joint location estimation and synchronization are achievable only with downlink MISO transmissions. Despite the fact that AOA method is not applied in MISO system, location estimation is still possible based on Angle of Departure (AOD) measurements [21], [22]. In this paper, we examine the impacts of hardware impairments on RIS-aided 3D drone localization as well as tracking. Our system incorporates a BS that transmits signals to the RIS units. The RIS then performs beam sweeping within the drone's area of interest. The localization process involves estimating the AOD from each RIS to the drone, and these AOD estimations are utilized in triangulation for three-dimensional (3D) drone localization and the Unscented Kalman Filter (UKF) for tracking.

### B. CONTRIBUTIONS OF THIS PAPER

The primary contributions of this paper include:

- Introducing an RIS-assisted drone localization system model, including an analysis of BS and RIS geometry on estimation performance with numerical results.
- Examining the effects of beam down-tilting from the BS to the RIS on AOD and 3D location accuracy.
- Demonstrating the principles of beam sweeping on the RIS for AOD estimation and the impact of the beam sweeping area on drone location accuracy.
- Modeling the phase noise (PN) on each element of the RIS and studying its impact on AOD and 3D location accuracy.
- Investigating the effects of system localization configuration, such as Inter-Site Distance (ISD), beam sweeping angle range, number of samples, and number of RIS elements.
- Validating AOD estimation performance by comparing the Cramér-Rao Lower Bound (CRLB) with the simulated variance of AOD estimation from the RIS to the drone.
- Validating the Position Error Bound (PEB) for 3D drone localization and evaluate the impact of the impairments.

### C. GOAL

The primary aim of this study is to estimate the location of a drone equipped with a single antenna, operating within a SISO system, and assisted by two RISs with hardware impairments. This is achieved by analyzing signals received at the drone from the BS via the RIS.

### D. ORGANIZATION OF THE PAPER

The detailed structure of this paper is organized as follows:

- Section II: This section introduces the general system model for localization, encompassing the configuration of the RIS, drone, and BS, alongside their channel modeling. It offers a comprehensive mathematical formulation for the RIS and discusses the localization impairments considered. Additionally, we outline the scope of the paper and the assumptions considered.

- Section III: Detailed in this section is the proposed methodology for drone localization. It covers beam sweeping techniques, AOA estimation, 3D location estimation, and employed tracking algorithm.
- Section IV: Evaluation of localization performance is presented here, with a particular focus on the CRLB in the context of hardware impairments at the RIS.
- Section V: This section shares our simulation results, discussing the location estimation performance under various scenarios, including those with and without impairments. The efficacy of the proposed methodology for drone localization is evaluated using multiple metrics.
- Section VI: This final section draws the main conclusions of the paper and outlines directions for future research.

## II. SYSTEM MODE

This section presents a model for RIS-assisted drone localization systems, as illustrated in Fig. 1. In this work, we emphasize the channel model from the BS to the RIS and from the RIS to the drone, taking into account the effects of hardware impairments on both the AOD and 3D drone location estimation.

### A. RIS-ASSISTED DRONE LOCALIZATION SCENARIO

We consider a drone localization and tracking system, as presented in Fig. 1, which consists of one BS positioned at a known location $\mathbf{B} = [b_x, b_y, b_z]^T$, equipped with a single antenna transmitter, and two RIS positioned at known 3D locations $(X_i, Y_i, Z_i)$, $i \in \{1, 2\}$. Each RIS is equipped with Uniform Planar Arrays (UPAs) of $\mathbf{M} = M_x \times M_y$ antenna elements, and the drone is mounted with a single antenna receiver at an unknown location. The BS communicates with the drone exclusively through the RIS. We assume the LoS path is obstructed. This scenario operates within a SISO system, featuring a single antenna at both the BS for transmission and the drone for reception.

### B. SIGNAL MODEL

In this work, we focus only on the non-line-of-sight (NLoS) path. As illustrated in Fig. 1, the drone receives signals from the two RIS via reflection from the RIS. The signal received $\mathbf{Y}_i$ at the drone can be modeled by the equation [23]:

$$\mathbf{Y}_i = \alpha_i \mathbf{H}_i^H \Phi_i \mathbf{G}_i \mathbf{S} + \mathbf{N}_i, \tag{1}$$

where $\mathbf{Y}_i \in \mathbb{C}^{N_r}$ is the signal received at the drone from the $i^{\text{th}}$ RIS ($i \in \{1, 2\}$), $\mathbf{S} \in \mathbb{C}^{N_t \times 1}$ is the signal transmitted from the BS, $\mathbf{G}_i \in \mathbb{C}^{M \times N_t}$ is the channel matrix from the BS to the $i^{\text{th}}$ RIS, $\mathbf{H}_i \in \mathbb{C}^{N_r \times M}$ is the channel matrix from the $i^{\text{th}}$ RIS to the drone, $\mathbf{N}_i \in \mathbb{C}^{N_r}$ represents the Additive White Gaussian Noise (AWGN) vector at the drone from the $i^{\text{th}}$ RIS. $\alpha_i$ is the complex channel gain for the paths via the $i^{\text{th}}$ RIS [24], [25].

The phase-shift matrix, with phase noise impairment, of $i^{th}$ RIS can be modeled as:

$$\Phi_i = \mathbf{\Theta}_i \hat{\Theta}_i \in \mathbb{C}^{M_i \times M_i}, \tag{2}$$

where $\mathbf{\Theta_i}$ represents the diagonal phase-shift matrix of the RIS, which can be written as:

$$\mathbf{\Theta}_i = \begin{bmatrix} \beta_1 e^{j[\vartheta_i]_1} & 0 & \cdots & 0 \\ 0 & \beta_2 e^{j[\vartheta_i]_2} & \cdots & 0 \\ \vdots & \vdots & \ddots & \vdots \\ 0 & 0 & \cdots & \beta_{M_i} e^{j[\vartheta_i]_{M_i}} \end{bmatrix} \in \mathbb{C}^{M_i \times M_i}, \tag{3}$$

In this model, $\vartheta_m$ represents the phase shift, and $\beta_m$ the reflection coefficient, of the $m^{th}$ antenna element within the RIS. We assume a constant reflection coefficient ($\beta_m = 1$), as supported by the research papers in [23], [26], and [27]. The phase noise for each element of the $i^{th}$ RIS is modeled as $\hat{\Theta}_i = \text{diag}\left(\left[e^{j[\phi_i]_1}, e^{j[\phi_i]_2}, \ldots, e^{j[\phi_i]_{M_i}}\right]\right)$, discussed in [28].

### C. CHANNEL MODEL

In this work, we consider a geometric channel model comprising angle of arrivals (AOAs) and angle of departures (AODs), along with the corresponding NLoS propagation paths [29]. This well-known channel parameter model is thoroughly discussed in [30] and [31]. The channel model $\mathbf{G}_i$, representing the channel from the BS to the RIS and defined in (1), is detailed as follows:

$$\mathbf{G}_i = \alpha_x(\theta_{t,i}, \phi_{t,i}) \otimes \alpha_y(\theta_{t,i}, \phi_{t,i}), \tag{4}$$

where $\mathbf{G}_i \in \mathbb{C}^{N \times 1}$ the array response vectors from the transmitting BS to the $i^{th}$ RIS, and the $\theta^1_{t,i}$ $\phi^1_{t,i}$, are the AOAs in elevation and azimuth of the $i^{th}$ RIS, respectively and it is represented in diagram in Fig.2. The corresponding array response vectors can be given as [32], [33]:

$$\alpha_x\left(\theta_{t,i}, \phi_{t,i}\right) = \begin{bmatrix} 1 \\ e^{j\frac{2\pi d_{1,x}}{\lambda}\cos(\theta_{t,i})\sin(\phi_{t,i})} \\ \vdots \\ e^{j\frac{2\pi d_{1,x}}{\lambda}(M_x-1)\cos(\theta_{t,i})\sin(\phi_{t,i})} \end{bmatrix},$$

$$\alpha_y\left(\theta_{t,i}, \phi_{t,i}\right) = \begin{bmatrix} 1 \\ e^{j\frac{2\pi d_{1,y}}{\lambda}\sin(\theta_{t,i})\sin(\phi_{t,i})} \\ \vdots \\ e^{j\frac{2\pi d_{1,y}}{\lambda}(M_y-1)\sin(\theta_{t,i})\sin(\phi_{t,i})} \end{bmatrix}, \tag{5}$$

where $M_x$ and $M_y$ denote the active antenna elements in the RIS across the $x$-axis and $y$-axis, respectively, and $d_{1,x}$ and $d_{1,y}$ represent their corresponding inter-space element.

Using similar concept given in (4), the channel from the RIS to the drone $\mathbf{H}_i$, can be also written as:

$$\mathbf{H}_i = \left[\alpha_x\left(\theta_{r,i}, \phi_{r,i}\right) \otimes \alpha_y\left(\theta_{r,i}, \phi_{r,i}\right)\right]^{\mathbf{H}}, \tag{6}$$

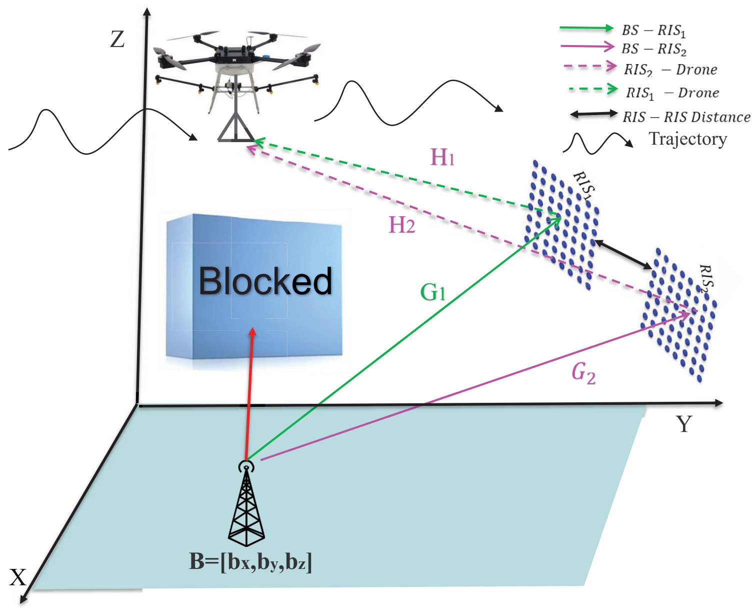


**FIGURE 1.** Physical illustration of the proposed RIS-assisted 3D drone localization model. The direct path from the BS to the drone is blocked.

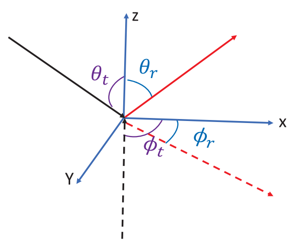


**FIGURE 2.** The AOAs (azimuth and elevation) arriving from the transmitting BS towards the RIS and the AOD (azimuth and elevation) originating from the RIS towards the drone.

where $\phi_{r,i}$, $\theta_{r,i}$ are the associated AODs in azimuth and elevation from the $i^{th}$ RIS towards the receiving drone. The other parameters are defined similarly to those described in (5).

### D. PROBLEM FORMULATION

Traditionally, GPS-based methods have been the standard for aeronautical system localization. However, the absence of a strong LoS communication link can cause GPS-based positioning to fail, a critical limitation that has garnered significant attention from wireless communication and positioning researchers. Solutions involving AOA, TOA, and Received Signal Strength (RSS) have been explored, all typically requiring extensive BS infrastructure. Yet, this infrastructure is particularly costly for drone localization in rural areas. In this paper, we introduce a RIS-assisted localization approach using a single BS and examine the impact of various impairments on drone localization and tracking performance.

### E. ASSUMPTIONS

- For simplicity, we assume the attenuation path loss from the BS transmitter to the RIS is negligible.
- The receiver has sufficient Signal-to-Noise Ratio (SNR).
- The beam sweeping speed is significantly faster than the speed of the drone.

### F. SCOPE OF THE STUDY

The scope of our study mainly focuses on:

- We consider 3.5 GHz frequency band as it is widely used for 5G whereas only very few operators have deployed mmWave and the current 5G mmWave beam tracking algorithm are not well suited for fast mobile users such as drone. It offers a good balance between coverage and capacity, making it suitable for both urban and suburban environments, particularly for drone communication and positioning.
- While there are existing studies on MIMO-based localization in RIS-aided systems [34], and leveraging localization for RIS-aided mmWave MIMO communications [35], in our study, we consider equipping the receiving drone with a single antenna due to its lightweight nature. To increase the gain from the BS to the RIS, we sectorized the antenna. Therefore, the focus of the paper is examining the introducing hardware imperfections at the RIS, and evaluate the impact of the drone location estimation within SISO configuration.
- We assume the drone is flying at a high altitude maintain LoS with the two RIS, thereby eliminating the effects of hills, obstacles, and multipath fading. In this work, we only consider the path loss associated with the

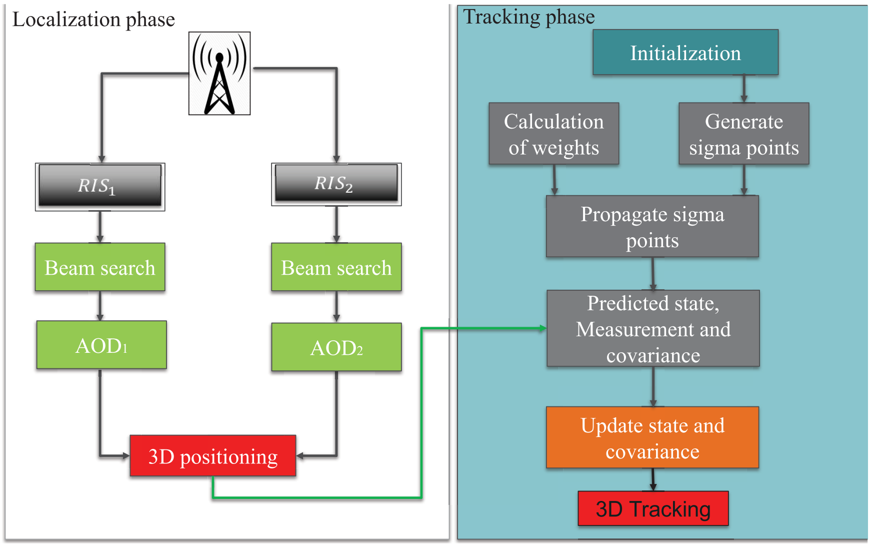


**FIGURE 3.** Flowchart of the proposed RIS-assisted 3D drone localization and tracking methodology, organized into two main phases: (i) the localization phase, which includes the estimation of AOD from the RIS to the drone (highlighted in green) and the estimation of the 3D drone position (indicated in red); (ii) the tracking phase, which utilizes the estimated 3D drone position as the measurement model for the UKF.

distance from the RIS to the drone. This assumption allows us to easily realize the impact of the introduced error.w

## III. PROPOSED DRONE LOCALIZATION METHOD

In this section, we outline the methodology employed in our research study, divided into two main phases. Initially, we model the channel path from the BS transmitter to the RIS, considering the effects of antenna downtilt and the associated AOAs. We then model the path from the RIS to the drone, incorporating the AODs from both RISs through exhaustive beam sweeping. Following this, we apply the half-line intersection method to estimate the drone's 3D position.

In the second phase, we examine the impact of the considered impairments on drone tracking. We apply the Unscented Kalman Filter (UKF) for drone tracking, processing each received signal. Here, the 3D location estimation serves as a measurement model for the tracking algorithm. A flow diagram illustrating this process is presented in Fig. 3.

### A. BS ANTENNA SECTOR

In this paper, we consider a single antenna at the BS that is sectorized in such a way that the main beam covers both RIS units. We measure the azimuth angles from the BS towards the two RIS units, aiming for improved antenna gain in their direction. The coverage of the sectored beam from the transmitting BS towards the two RIS, along with the red and black asterisks marking the positions of the first and second RIS at 106° and 79°, respectively, relative to the BS transmitter, is illustrated in Fig. 4. Once the main beam from the BS to the RIS is appropriately sectorized, we examine the impact of beam downtilting at various elevations on the accuracy of AOD estimation from the RIS to the drone. Contour plots in Fig. 4 demonstrate how the beam pattern from the BS transmitter to the RIS is affected by downtilt in the elevation angle. It is observed that further downtilting of the beam results in decreased gain at the RIS, which makes the AOD estimation worsen.

### B. AOD ESTIMATION

After the signal is emitted from the transmitting BS to the RIS, the channel matrix or gain $G_i$ can be modeled given the known locations of the transmitter and the RIS. The signal reflection towards the drone is optimized by adjusting the phase shifts of the RIS elements to enhance signal reception. To maximize the received signal at the drone, optimal phase shifts for each RIS element are determined through beam sweeping [36], aiming to optimize the model described by (1). This process is mathematically represented as:

$$(\hat{\theta}, \hat{\phi}) = \arg\max_{\theta,\phi} \|\mathbf{Y}_i\|^2, \tag{7}$$

where $\|\mathbf{Y}_i\|^2$ denotes the norm squared of the received signal at the drone from the $i^{th}$ RIS. Here, $\hat{\theta}$ and $\hat{\phi}$ are the estimated elevation and azimuth angles corresponding to the peak received signal, representing the AOD from the RIS towards the drone.

In this paper, we have applied beam sweeping in both azimuth and elevation from the RIS to the drone, utilizing a predefined set of angles for beam sweeping [19]. After performing exhaustive beam sweeping, the drone estimates the index of the beam signal with the highest reception from each RIS. For simplicity purpose, we assume identical angle steps for sweeping in both azimuth and elevation. The

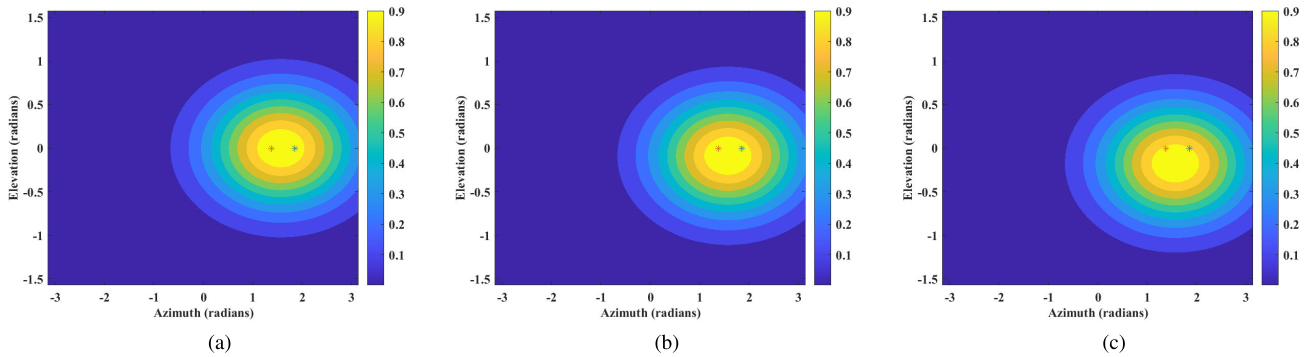


**FIGURE 4.** Three contour representing radiation pattern of the BS transmitter towards the RIS in azimuth and elevation under three beam tilt conditions. The plots in a). down-tilting with $0^o$, b). down-tilting with $5^o$ and c). down-tilting with $10^o$.

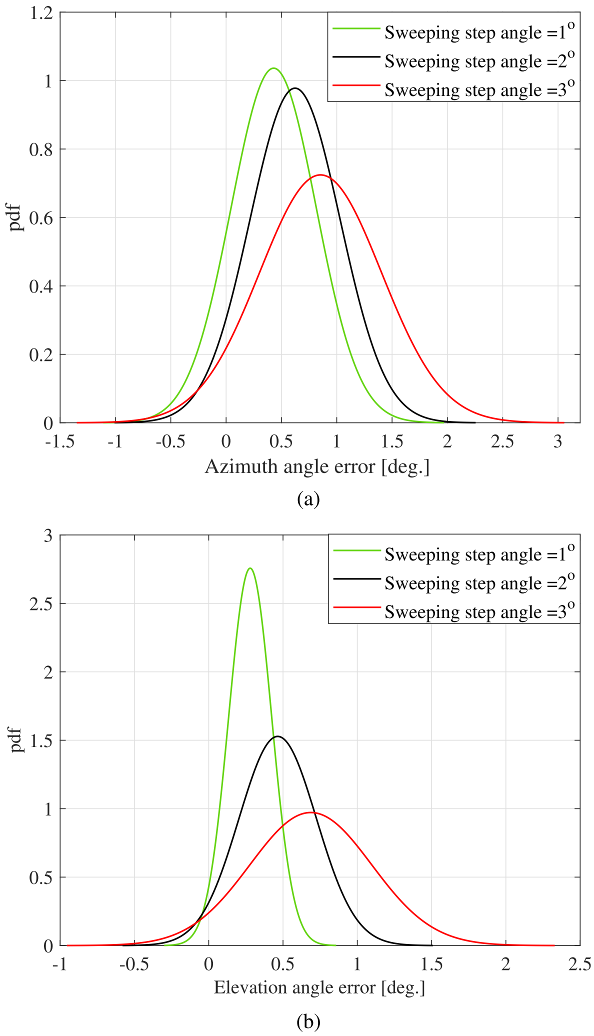


**FIGURE 5.** Impact of sweeping angle steps on AOD estimation for the drone from the first RIS at [20, 100, 3]: (a) Azimuth estimation; (b) Elevation estimation.

solution to the problem defined in (7) yields the estimated AOD in terms of azimuth and elevation angles. The impact of the sweeping step angle, in the absence of any impairments, is illustrated in Fig.5.

### *C. LOCATION ESTIMATION*

Once the AODs in both azimuth and elevation angles are estimated, the next step involves computing the 3D location estimation based on the 3D AOD and the known location information of the RIS. The 3D location of the drone can be estimated using either the intersection or the Least Squares (LS) method, both of which are applied to the two half-lines that extend from each RIS towards the drone.

After estimating the AODs from both RIS using exhaustive beam sweeping, we employed the intersection of lines based on the known RIS locations and the estimated AOD at the drone. Let the coordinates $(X_i, Y_i, Z_i)$, $i \in (1, 2)$ represent the known locations of the stationary, identical RIS, and let $\hat{\theta}_{i,k}$ and $\hat{\phi}_{i,k}$ respectively denote the estimated elevation and azimuth angles from the RIS to the drone over time. Let $(x_k, y_k, z_k)$ represent the unknown coordinates of the hovering drone at time $k$, where $k$ denotes the sampling time.

The 3D position of the drone can be estimated using the AODs from both stationary RIS to the drone and the 3D positions of the RIS. As shown in Fig. 1, the 3D position of the drone can be estimated from the lines through the two RIS, $R_i$, in the direction of $(\hat{\theta}_{i,k}, \hat{\phi}_{i,k})$ in a spherical coordinate system. We can formulate two half-line functions from the two RIS towards the drone in 3D space, and the intersection of these lines provides the estimated 3D location of the drone.

To define the direction of the reflected signal from the RIS, let us express it using Cartesian coordinates:

$$\begin{bmatrix} x_{i,k} \\ y_{i,k} \\ z_{i,k} \end{bmatrix} = \begin{bmatrix} \cos(\hat{\theta}_{i,k})\cos(\hat{\phi}_{i,k}) \\ \cos(\hat{\theta}_{i,k})\sin(\hat{\phi}_{i,k}) \\ \sin(\hat{\theta}_{i,k}) \end{bmatrix}, \tag{8}$$

and we can formulate the line from the first RIS $(X_1, Y_1, Z_1)$ to the unknown 3D position of the drone in parametric form:

$$\frac{x_k - X_1}{a_1} = \frac{y_k - Y_1}{a_2} = \frac{z_k - Z_1}{a_3} = t, \tag{9}$$

where $a_1, a_2, a_3$ are the direction vectors toward the drone, and $t$ is a parameter describing a point on the line.

Considering again the second RIS $(X_2, Y_2, Z_2)$, we have a symmetrical relation:

$$\frac{x_k - X_2}{b_1} = \frac{y_k - Y_2}{b_2} = \frac{z_k - Z_2}{b_3}, \quad (10)$$

where $b_1, b_2$, and $b_3$ are the direction vectors from the second RIS toward the estimated 3D location of the drone. By substituting (10) into (9) and solving for $t$, the estimated 3D position of the drone is evaluated in the Cartesian coordinate.

### D. TRACKING WITH UNSCENTED KALMAN FILTER

The noise of Gaussian processes can be characterized by random variables that follow normal distribution functions. Typically, the Kalman filter is employed to track the state of linear systems because it provides optimal estimation in environments where the processes are linear and the noise is Gaussian [37]. However, Kalman filter is not suitable for nonlinear system models, which yields to the development of the EKF to address this limitation. The EKF approximates the nonlinear model as a Gaussian random variable with first-order Taylor series method of linearizing during its prediction process. However, for systems with significant nonlinearity, this approximation can introduce substantial noises in the estimated posterior mean and covariance, ultimately diminishing the accuracy of the tracking performance [38]. Despite the limitations in estimation accuracy, we applied a combination of MUSIC and EKF for positioning and tracking respectively, as detailed in our previous papers [18], [39].

The algorithm of Unscented Kalman Filter (UKF) employs the Unscented Transform (UT), a stochastic linearization technique that uses a weighted statistical linear regression approach. Within this transformation, the selection of sigma points is fundamental, as they are instrumental in capturing true mean and covariance of the probability distribution for more accurate state estimation [40]. In this paper, we present a model where the drone's trajectory is a nonlinear function varying in three-dimensional space over time. We assume the estimated three dimensional location from the RIS to be the measurement model utilized by the UKF. Tracking using UKF involve two main steps described below.

#### 1) UKF ALGORITHM

Consider the following nonlinear system equations:

$$\left.\begin{aligned} x_k &= f(x_{k-1}, u_k) + w_{k-1} \\ y_k &= h(x_k) + v_k \end{aligned}\right\} \quad (11)$$

where $f(,)$ and $h(,)$ represent the nonlinear function, and $x_k$, $u_k$ and $y_k$ represent the state vector, the input and output vectors at time instant $k$, respectively. $w_k$ and $v_k$ are the process noise and measurement noise that are not correlated,respectively. In this paper, we follow the UKF algorithm explained in [41] and [42]. Let us consider each step separately.

##### a: SIGMA POINTS GENERATION STAGE

The use of generating sigma points is to estimate accurately the mean and covariance of the state estimate. These points are selected from the mean to the left and right with the same distance in the axis.

$$\begin{aligned} \chi_{k-1} = [&\hat{x}_{k-1}, \\ &\hat{x}_{k-1} + (\sqrt{(\lambda + L)P_{k-1}})_i, \; i = 1, \ldots, L \\ &\hat{x}_{k-1} - (\sqrt{(\lambda + L)P_{k-1}})_i, \; i = L+1, \ldots, 2L] \end{aligned} \quad (12)$$

where $\hat{x}_{k-1}$ represents the state estimate, $P_{k-1}$ denotes the covariance of the state estimate, respectively. The $L$ and $\lambda$ are the dimension of the state and scaling parameter, respectively.

##### b: PREDICTION STAGE

This stage has two main steps. First, the generated sigma points are propagated through the nonlinear state function:

$$\chi_{k|k-1} = f(\chi_{k-1}, \mathbf{u}_{k-1}), \quad (13)$$

to predict the next state sigma points.

The second step involves computation of the predicted state mean and covariance as:

$$\hat{x}_k^- = \sum_{i=0}^{2L} W_i^m \chi_{k|k-1}^i, \quad (14)$$

$$P_{x_k}^- = \sum_{i=0}^{2L} W_i^c \left(\chi_{k|k-1}^i - \hat{x}_k^-\right)\left(\chi_{k|k-1}^i - \hat{x}_k^-\right)^T + Q_k, \quad (15)$$

where $W_i^{(m)}$ and $W_i^{(c)}$ defines the weights for the mean and covariance, respectively, and $Q_k$ is the process noise covariance.

##### c: UPDATE STAGE

This stage also has two main steps. The first step involves propagating the sigma points through the measurement model to predict the measurement:

$$Z_{k|k-1} = h(\chi_{k|k-1}), \quad (16)$$

$$\hat{z}_k^- = \sum_{i=0}^{2L} W_i^m Z_{k|k-1}^i. \quad (17)$$

$$K_k = P_{x_k z_k} P_{z_k z_k}^{-1}, \quad (18)$$

$$\mathbf{x}_{k|k} = \hat{x}_k^- + K_k(\mathbf{z}_k - \hat{z}_k^-), \quad (19)$$

$$P_{k|k} = P_{x_k}^- - K_k P_{z_k z_k} K_k^T. \quad (20)$$

The second step in the UKF update process involves updating the state estimate and covariance with the actual measurement. To compute the kalman gain, we need first to calculate cross-covariance matrix and measurement prediction covariance separately. The cross-covariance matrix $P_{x_k z_k}$ presents the correlation between the state and measurement predictions,given as follows:

$$P_{x_k z_k} = \sum_{i=0}^{2L} W_i^c (\chi_{k|k-1}^i - \hat{x}_k^-)(Z_{k|k-1}^i - \hat{z}_k^-)^T, \quad (21)$$

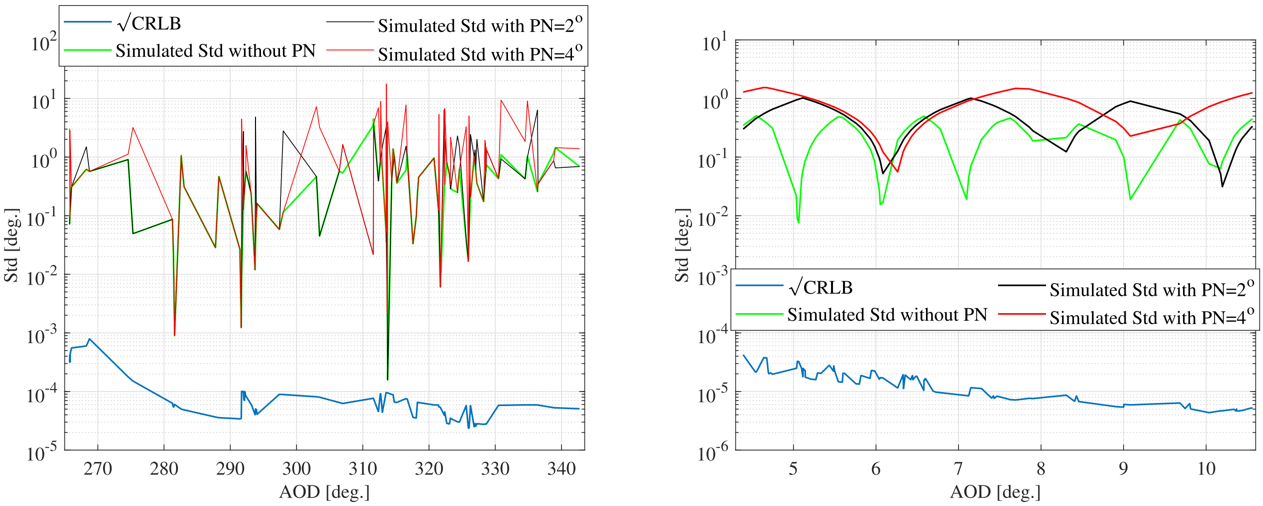


(a) (b)

**FIGURE 6. Comparison of the CRLB and the simulated variance of AOD estimates under phase noise impairments, given the parameters ($N_t = 1$, representing a single transmitter antenna; $M = 100$, denoting the number of reflecting elements; $ISD = 80$ meters; $d = 0.5\lambda$, with $\lambda$ being the wavelength): (a). azimuth CRLB; (b). elevation CRLB.**

where $\chi^i_{k|k-1}$ are the generated sigma points for the state at time step $k$ predicted from time step $k-1$, $Z^i_{k|k-1}$ also denote the sigma points for the measurement predicted from the state predictions, $\hat{x}^-_k$ is the predicted state vector, $\hat{z}^-_k$ is the predicted measurement vector.

The measurement prediction covariance $P_{z_k z_k}$ also shows the expected accuracy of the measurement predictions, which is computed as:

$$P_{z_k z_k} = \sum_{i=0}^{2L} W^c_i (Z^i_{k|k-1} - \hat{z}^-_k)(Z^i_{k|k-1} - \hat{z}^-_k)^T + R_k, \quad (22)$$

where $R_k$ is the measurement noise covariance matrix at time $k$. The Kalman gain, the estimated state, and the covariance matrix are given, respectively, as follows:

## IV. LOCALIZATION PERFORMANCE BOUNDS

The accuracy of AOD and 3D position estimation is crucial for evaluating localization performance. The effectiveness of the employed estimation algorithm can be assessed by comparing the estimates with ground truth and analyzing the variance of these estimates. The CRLB is defined as a lower bound on the variance, or mean square error (MSE), of any unbiased estimator of a parameter, such as angle and location. It can be expressed as the inverse of the Fisher Information Matrix (FIM). Hence, to assess the accuracy of AOD estimates from the two RIS to the drone, we employ the derived expressions for the FIM for both angle and position estimates, as discussed in [43] and [44].

### A. CRLB ANALYSIS FOR AoA ESTIMATION

The channel AOD estimation state–vector at the $i^{th}$ RIS at time–step $k$, denoted by $\boldsymbol{\zeta}^i_k \in \mathbb{R}^2$, can be written as [43], [45]:

$$\boldsymbol{\zeta}^i_k = \begin{bmatrix} \theta^i_k & \phi^i_k \end{bmatrix}^T. \quad (23)$$

Given the signal model, the general deterministic CRLB on the covariance matrix of unbiased channel parameter estimator of $\boldsymbol{\zeta}$ is given as:

$$\mathbf{CRLB}_{\zeta} = \frac{\sigma^2_w}{2} \left\{ \Re \left\{ \boldsymbol{S}^\dagger \boldsymbol{D}^\dagger \boldsymbol{\Pi}^\perp_A \boldsymbol{D} \boldsymbol{S} \right\} \right\}^{-1}, \quad (24)$$

where $\Pi^\perp_A$ denotes the projection onto nullspace of $A$ represented as $\Pi^\perp_A = \boldsymbol{I} - \boldsymbol{A}(\boldsymbol{A}^\dagger \boldsymbol{A})^{-1} \boldsymbol{A}^\dagger$, and $\boldsymbol{A}$ represents the beampattern of $m$ far–field sources, and $\boldsymbol{D}$ also denotes the partial derivative of steering vector $A$ with respect to $\boldsymbol{\zeta}$, both expressed as:

$$\boldsymbol{A} = [\boldsymbol{a}(\theta_1, \phi_1), \boldsymbol{a}(\theta_2, \phi_2, ), \ldots, \boldsymbol{a}(\theta_m, \phi_m)], \quad (25a)$$
$$\boldsymbol{D} = [\boldsymbol{a}'_1, \boldsymbol{a}'_2, \ldots, \boldsymbol{a}'_m], \quad (25b)$$

where $\boldsymbol{a}'_m = \frac{\partial \boldsymbol{a}_m}{\partial \theta_m}$.

Fig. 6 illustrates the CRLB for AOD in azimuth and elevation, calculated using (24), and compares it with the simulated sample variance of AOD estimation for the second RIS, both with and without PN impairments. This plot shows how AOD estimation variance, in both azimuth and elevation, fluctuates with each drone movement within the area of interest. Variance is affected by the random generation of Gaussian noise and the varying signals transmitted from the BS, which change with each drone movement. Consequently, the variance of AOD estimation differs each time the drone receives the reflected signal from the RIS, showing the dynamic nature of AOD estimation under the simulation parameters.

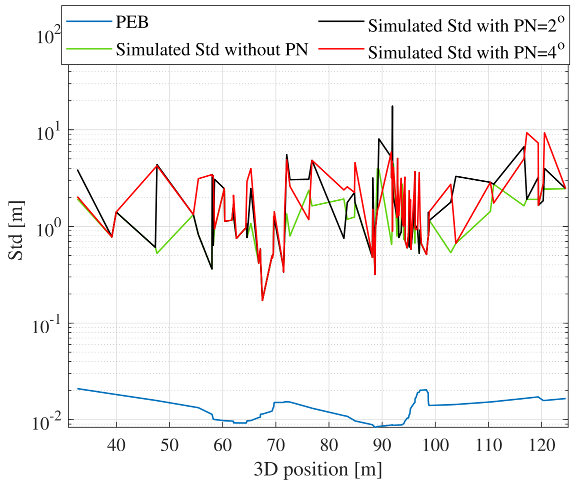


**FIGURE 7.** Comparison of the PEB and the simulated variance of 3D drone positioning estimates under phase noise impairments.

### B. POSITION ERROR BOUND (PEB) ANALYSIS

Let $(x_i, y_i, z_i)$ denote the coordinates of the $i^{th}$ RIS as seen from the $k^{th}$ position of the drone, whose orientation is known with respect to a reference point at the origin. The state vector of the drone is given as:

$$\boldsymbol{p}_k = [X_k, Y_k, Z_k]^T \tag{26}$$

The least squares estimator, which relates measurements and parameters of interest non-linearly, is defined as follows:

$$\boldsymbol{r}_i = \left[\arctan\left(\frac{y_i - Y_k}{x_i - X_k}\right), \ \arctan\left(\frac{z_i - Z_k}{d_{ki}^{2D}}\right)\right]^T \tag{27}$$

where $d_{ki}^{2D} = \sqrt{(x_i - X_k)^2 + (y_i - Y_k)^2}$ is the 2D distance between the drone and the $i^{th}$ RIS in the $xy$ plane. The deterministic CRLB on the covariance matrix of an unbiased position estimator of $\boldsymbol{p}_k$ is given as [15], [46], [47], [48]:

$$\boldsymbol{CRB}_{\boldsymbol{p}_k} = \frac{\sigma_w^2}{2}\left(\left(\frac{\partial \boldsymbol{r}_i}{\partial \boldsymbol{p}_k}\right)^{\dagger}\left(\mathcal{Q}_i^{[k]}\right)^{-1}\frac{\partial \boldsymbol{r}_i}{\partial \boldsymbol{p}_k}\right)^{-1} \tag{28}$$

The Position Error Bound (PEB) can then be derived from the CRLB as:

$$\mathrm{PEB}_k = \sqrt{\mathrm{trace}(\boldsymbol{CRB}_{\boldsymbol{p}_k})} \tag{29}$$

## V. SIMULATION RESULTS AND DISCUSSIONS

In this section, we introduce the simulation setup, including the configuration of the BS, the RIS, and trajectory of the drone. We also present numerical results to demonstrate the performance of the proposed localization and tracking approach, and discuss the impact of impairments on angle and location estimation accuracy.

### A. SIMULATION SETUP

To assess the performance of RIS-assisted drone localization, we established a simulation environment as shown in Fig. 9.

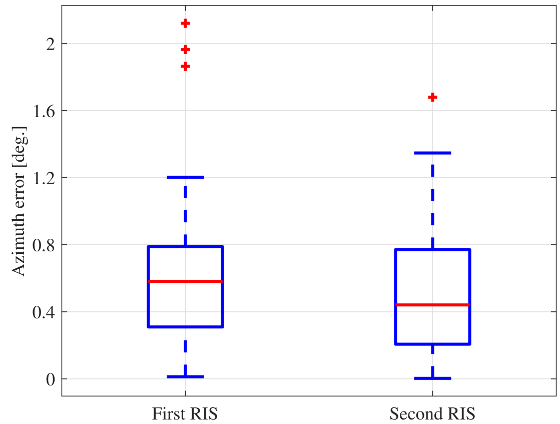


(a)

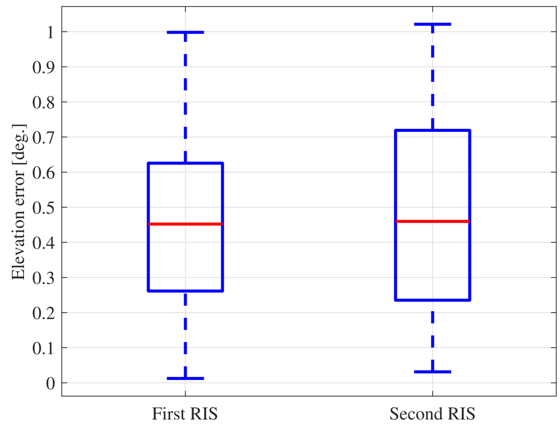


(b)

**FIGURE 8.** Simulation results for AOD accuracy without impairments for both RIS, with parameters set to $N_t = 1$, $M = 100$, $ISD = 80$ meters, and $d = 0.5\lambda$: (a) azimuth estimation accuracy; (b) elevation estimation accuracy.

**TABLE 1.** Main simulation parameters.

| Parameter | Symbol | Value |
|---|---|---|
| Carrier frequency | $f_c$ | 3.5 GHz |
| BS transmission power | $P_t$ | 20 dBm |
| Number of antenna in BS | $N_t$ | 1 |
| Number of elements in RIS | $M$ | 100 |
| Number of receive antenna | $N_r$ | 1 |
| Height of BS | $H_{BS}$ | 3 $m$ |
| Height of drone | $H_{UAV}$ | 6-12 $m$ |
| Height of IRS center | $H_{IRS}$ | 3m |
| Distance between BS and IRS | $L$ | 80m |

The BS and two RISs are positioned at coordinates (50, 0, 3) meters, (20, 100, 3) meters, and (80, 100, 3) meters, respectively. To examine the impact of varying ISD between the RISs on estimation accuracy, we positioned the RISs at ISDs of 80 $m$, 100 $m$, and 140 $m$, analyzing the effects on angle and location accuracy. The simulation parameters are detailed in Table 1.

### B. AOD ESTIMATION PERFORMANCE

In this section, we assess the AOD estimation accuracy from both RIS units. Given that the precision of 3D location

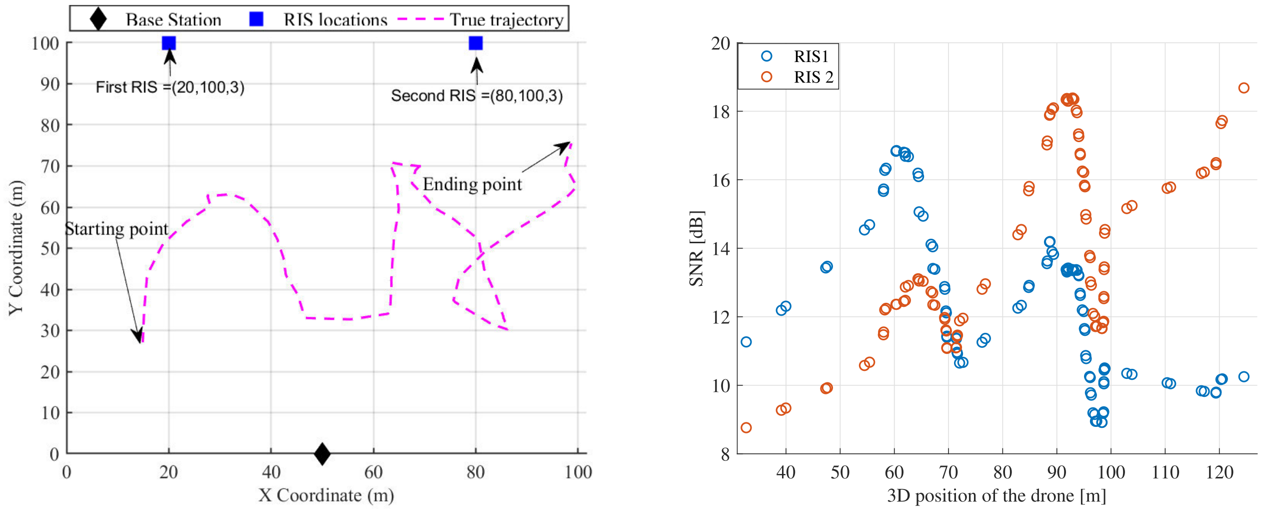


(a) (b)

**FIGURE 9. The simulation setup for SISO RIS-assisted drone positioning employing a BS transmitter with $N_t$ antennas, a RIS of dimensions $M_r \times M_c$, and a drone equipped with an $N_r$ antenna receiver; (a). Position of the two RISs, BS and actual drone trajectory; (b). SNR values at the drone in its different 3D positions.**

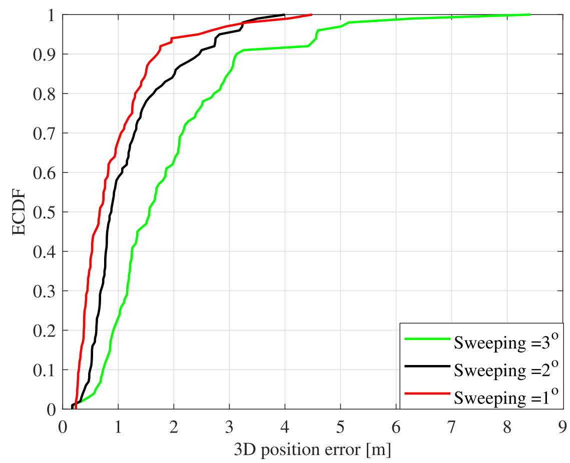


**FIGURE 10. CDF plots depicting the impact of beam sweeping angle increments on the accuracy of 3D localization evaluation. Parameters are set to $N_t = 1$, $M = 100$, $ISD = 80$, $d = 0.5\lambda$.**

estimation for the drone is largely contingent upon the resolution of the AOD estimation, we initially determine the azimuth and elevation angles from both RIS units in relation to the drone. We quantify the accuracy by evaluating the absolute deviation between the estimated AOD and the ground truth, which is derived from the drone's actual trajectory.

The AOD estimation results for both RIS units are depicted in Fig. 8. These results indicate the potential for a maximum estimation error of up to $2^o$ in azimuth and up to $1^o$ in elevation for both RIS units. These results are without impairments and with the simulation parameters given in Fig. 8. Fig. 9b shows the SNR at the drone as a function of the distance from the drone to the RIS locations. It can be observed that the SNR decreases as the distance from the drone to each RIS increases.

### C. POSITIONING PERFORMANCE EVALUATION

In this section, we will discuss the impact of some some parameters on localization and tracking algorithm performance. Such as the ISD between the two RIS, PN at each antenna elements of the RIS, down tilting the main beam from the BS to the RIS, step size of beam sweeping.

In this section, numerical results are provided to evaluate the performance of RIS aided drone localization and tracking for a given impairments.

#### 1) IMPACT OF STEP ANGLE OF BEAM SWEEPING

The performance of RIS-assisted localization also depends on the angle sweeping steps from the RIS towards the drone equipped with receiver. In this section, we conducted our simulation with different angle step sizes and evaluate the 3D drone positioning. The CDF plot shown in Fig. 10, demonstrates 90% of the distribution accuracy of 1.92 *m*, 2.83 *m*, 4.5 *m* for sweeping a angles 1°, 2°, 3° respectively.

#### 2) IMPACT OF NUMBER OF ELEMENTS ON THE ACCURACY

The number of elements used to construct the RIS can significantly impact the accuracy of location estimation. Therefore, we investigate the performance of our approach with respect to different numbers of antenna elements in the RIS. As demonstrated in Fig. 11, we can achieve the $90^{th}$ percentile error of 4.5 *m* with only 64 elements arranged in a square configuration. In contrast, by increasing the number of antenna elements in the RIS to 100 and 144, we achieve $90^{th}$ percentile errors of approximately 2.7 *m* and 2.4 *m*,

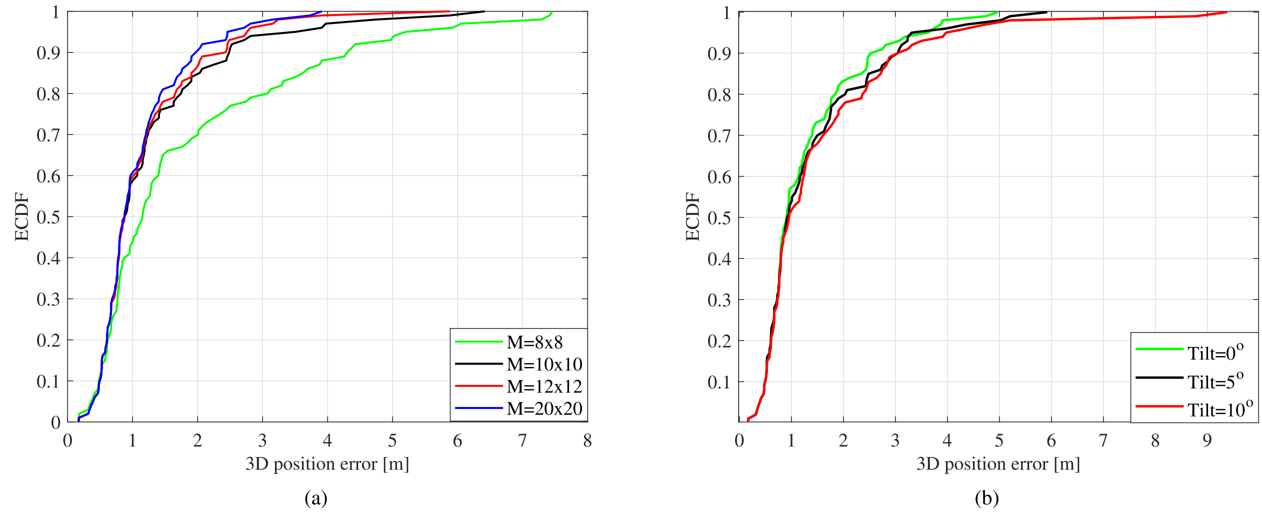


**FIGURE 11.** CDF plots presenting the impact of impairments on the accuracy of 3D localization evaluation, with parameters set to: $N_t = 1$, $ISD = 80m$, $d = 0.5\lambda$. (a). Effects of the number of elements at the RIS; (b). Effect of beam tilting at the BS transmitter.

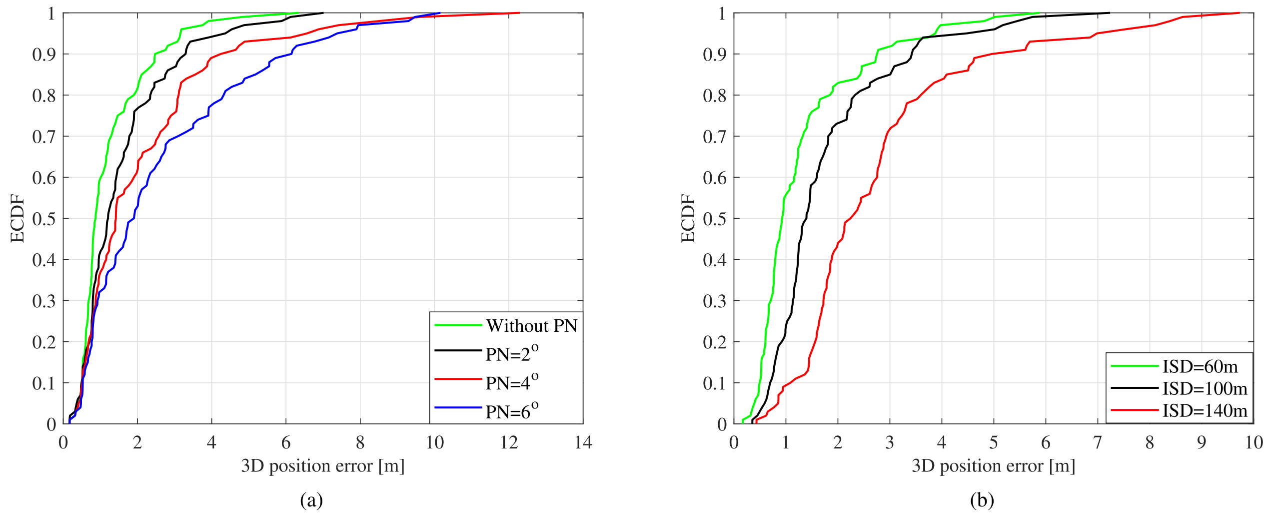


**FIGURE 12.** CDF plots depicting the impact of impairments on the accuracy of 3D localization evaluation, with parameters set to: $N_t = 1, M = 100$, $ISD = 80m$, $d = 0.5\lambda$. (a). Influence of the PN at the elements of the RIS; (b). Effect of ISD between the two RIS.

respectively. It can be concluded that location estimation accuracy improves with the increasing antenna elements in the RIS.

### 3) IMPACT OF ANTENNA TILTING

In this paper, we equip the BS transmitter with a single antenna and increase the gain of the transmitting antenna towards the RIS by sectorizing it. This sectorization ensures that the two RISs units are covered by the sectored beam, as shown in Fig. 4. To study the impact of antenna tilting on location accuracy, we tilt the main transmitter beam and evaluate the localization performance under different tilt values. Fig. 4 presents the effect of downward tilting of the main beam on the coverage of the two RIS units.

Fig. 11b displays the localization accuracy of a system without beam tilting, where 90% of the position errors are less than 2.5 $m$. However, introducing a $5^o$ beam tilt and a $10^o$ beam tilt results in 90% accuracy dropping to under 3.0 $m$ and 3.4 $m$, respectively. This comparative analysis demonstrates that greater beam tilting angles lead to diverge in localization performance.

### 4) IMPACT OF PHASE NOISE

In this paper, we also consider the impact of phase noise on RIS-assisted SISO localization. We introduce phase noise at each elements of the RIS and evaluate its effect on the AOD and the accuracy of 3D location estimation. As the beam sweeping covers a range of directions, the impact of phase noise on any single antenna is insignificant or minimized when considering the overall beam pattern. The CDF plot shown in Fig. 12 demonstrates that the effect of phase noise on 3D location accuracy is minimal. Any small impact that

**TABLE 2.** $90^{th}$ **Percentile of AOD, 3D positioning (m) and tracking (m) errors under different impairments.**

| $i^{th}$ RIS | | PN [deg.] | | | Tilt [deg.] | | | Sweeping [deg.] | | | M | | |
|---|---|---|---|---|---|---|---|---|---|---|---|---|---|
| | | 0 | 2 | 4 | 0 | 5 | 10 | 1 | 2 | 3 | 64 | 100 | 144 |
| $1^{st}$ RIS | Azimuth | 1.4 | 1.5 | 2.45 | 1 | 1.25 | 1.5 | 1.2 | 1.4 | 1.6 | 1.8 | 1.6 | 1.45 |
| | Elevation | 1.251 | 1.05 | 0.97 | 0.95 | 0.95 | 0.97 | 0.65 | 0.85 | 1.37 | 0.95 | 0.96 | 0.81 |
| $2^{nd}$ RIS | Azimuth | 0.9 | 1.5 | 2.2 | 0.9 | 1.1 | 1.3 | 0.8 | 0.9 | 1.5 | 1.6 | 1.2 | 0.8 |
| | Elevation | 0.95 | 0.96 | 0.98 | 0.8 | 0.83 | 0.87 | 0.67 | 0.96 | 1.44 | 1.3 | 1.3 | 0.75 |
| Positioning | | 3.1 | 4 | 6 | 2.1 | 3 | 3.4 | 2.8 | 3.5 | 5 | 4 | 3.20 | 2.5 |
| Tracking | | 3.0 | 3.8 | 5.8 | 2.30 | 2.95 | 3.0 | 3.08 | 3.3 | 4.7 | 3.8 | 3.20 | 2.6 |

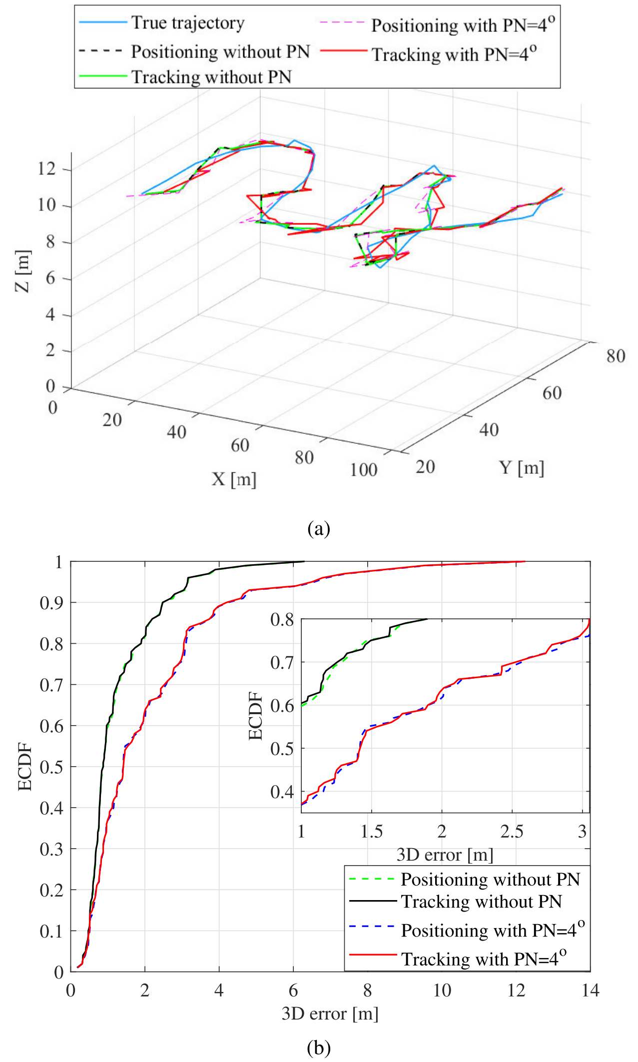


**FIGURE 13.** **CDF plot for evaluating the accuracy of drone positioning and tracking in simulations, with parameters set as follows:** $N_t = 1$, $ISD = 80$, $M = 100$, **and** $d = 0.5\lambda$.**(a) shows a comparison between the true 3D trajectory and the estimated paths, with and without phase noise (PN). (b) presents the CDF of positioning and tracking accuracy under scenarios with and without PN.**

does occur is due to the random noise inherent in the signal and noise.

#### 5) IMPACT OF ISD BETWEEN THE RIS

We consider flying the drone with 3D positional variation over time, starting from a height of 10 $m$ above the ground and descending to 6 $m$. We observe the effect of the ISD between the two RISs on the the accuracy of 3D drone position estimation.

The CDF shown in Fig. 12b depicts the impact of the ISD between the two RIS units on the accuracy of drone location estimation. With ISDs set at 60 $m$, 100 $m$, and 140 $m$, the $90^{th}$ percentile of 3D drone location accuracy is achieved at 2.5 $m$, 3.5 $m$, and 5 $m$, respectively.

The $90^{th}$ percentile errors for the AOD in azimuth and elevation, 3D location, and tracking for both RIS units are provided in Table 2.

### D. TRACKING PERFORMANCE EVALUATION

After evaluating the performance of our proposed RIS-assisted drone localization approach, we implemented the UKF algorithm to track the drone at each sampling point during signal reception. The 3D location, estimated from the information of the estimated AOD and the known RIS location, was used as the measurement model for the UKF algorithm. The 3D plot in Fig.13a presents the true trajectory with the estimated 3D position and tracking, demonstrating that the positioning and tracking without PN closely follow the true trajectory. But, the positioning and tracking with PN has a some diverges.

In the 3D plot shown in Fig. 13a, we can observe that, although there are minor divergences in some parts of the trajectory with PN, the majority of the trajectory closely follows the true trajectory. This can be seen in the CDF plot in Fig. 13b, where the positioning and tracking accurately reflect the true trajectory of the drone.

Fig.13 illustrates the positioning and tracking errors both with and without phase noise, demonstrating that a median error of less than 1 $m$ can be achieved in both positioning and tracking in the absence of phase noise. With phase noise, the median error remains less than 2 $m$.

## VI. CONCLUSION

This paper has investigated a wireless 3D drone localization and tracking system through simulation, employing a SISO system assisted by two RISs at known positions. Our study builds on existing RIS-assisted localization research, filling the gap where hardware impairments have not been thoroughly considered. We have shown that hardware impairments influence the accuracy of RIS-aided 3D drone localization and tracking, providing insights into navigating these challenges.

Extensive simulations have revealed that high accuracy in both AOD estimation and 3D drone localization and tracking is achievable. Despite substantial ISD between RISs, and potential hardware impairments such as phase noise on RIS elements and downtilt at the BS, a RIS-assisted localization system can still achieve reasonable accuracy. Specifically, considering PN impairments,We demonstrated that the 3D location median error is approximately less than 2 meters for all the considered phase noise levels These outcomes affirm that high-probability 3D positioning accuracy is feasible, even with impairments, within an RIS-assisted drone localization system. Moving forward, further exploration into practical RIS-assisted drone localization could yield additional insights, setting the stage for real-world applications of our findings.

## REFERENCES

[1] M. Meles, A. Rajasekaran, K. Ruttik, R. Virrankoski, and R. Jäntti, "Measurement based performance evaluation of drone self-localization using AoA of cellular signals," in *Proc. 24th Int. Symp. Wireless Pers. Multimedia Commun. (WPMC)*, Dec. 2021, pp. 1–5.

[2] P. Nguyen, T. Kim, J. Miao, D. Hesselius, E. Kenneally, D. Massey, E. Frew, R. Han, and T. Vu, "Towards RF-based localization of a drone and its controller," in *Proc. 5th Workshop Micro Aerial Vehicle Netw., Syst., Appl.*, Jun. 2019, pp. 21–26.

[3] J. Zhang, R. Xi, Y. He, Y. Sun, X. Guo, W. Wang, X. Na, Y. Liu, Z. Shi, and T. Gu, "A survey of mmWave-based human sensing: Technology, platforms and applications," *IEEE Commun. Surveys Tuts.*, vol. 25, no. 4, pp. 2052–2087, 1st Quart., 2023.

[4] J. Zhang, X. Na, R. Xi, Y. Sun, and Y. He, "MmHawkeye: Passive UAV detection with a COTS mmWave radar," in *Proc. 20th Annu. IEEE Int. Conf. Sens., Commun., Netw. (SECON)*, Sep. 2023, pp. 267–275.

[5] A. Taffanel. *Loco Positioning System*. Bitcraze.io. Accessed: Mar. 10, 2024. [Online]. Available: https://www.bitcraze.io/documentation/system/positioning/loco-positioning-system

[6] G. C. Alexandropoulos, G. Lerosey, M. Debbah, and M. Fink, "Reconfigurable intelligent surfaces and metamaterials: The potential of wave propagation control for 6G wireless communications," 2020, *arXiv:2006.11136*.

[7] H. Wymeersch, J. He, B. Denis, A. Clemente, and M. Juntti, "Radio localization and mapping with reconfigurable intelligent surfaces: Challenges, opportunities, and research directions," *IEEE Veh. Technol. Mag.*, vol. 15, no. 4, pp. 52–61, Dec. 2020.

[8] H. Chen, H. Kim, M. Ammous, G. Seco-Granados, G. C. Alexandropoulos, S. Valaee, and H. Wymeersch, "RISs and sidelink communications in smart cities: The key to seamless localization and sensing," 2023, *arXiv:2301.03535*.

[9] S. Eddine Zegrar, L. Afeef, and H. Arslan, "A general framework for RIS-aided mmWave communication networks: Channel estimation and mobile user tracking," 2020, *arXiv:2009.01180*.

[10] M. Di Renzo, F. Habibi Danufane, X. Xi, J. de Rosny, and S. Tretyakov, "Analytical modeling of the path-loss for reconfigurable intelligent surfaces—Anomalous mirror or scatterer ?" in *Proc. IEEE 21st Int. Workshop Signal Process. Adv. Wireless Commun. (SPAWC)*, May 2020, pp. 1–5.

[11] A. Bourdoux, A. Noll Barreto, B. van Liempd, C. de Lima, D. Dardari, D. Belot, E.-S. Lohan, G. Seco-Granados, H. Sarieddeen, H. Wymeersch, J. Suutala, J. Saloranta, M. Guillaud, M. Isomursu, M. Valkama, M. Reza Kahar Aziz, R. Berkvens, T. Sanguanpuak, T. Svensson, and Y. Miao, "6G white paper on localization and sensing," 2020, *arXiv:2006.01779*.

[12] H. Wymeersch, J. He, B. Denis, A. Clemente, and M. Juntti, "Radio localization and mapping with reconfigurable intelligent surfaces," 2019, *arXiv:1912.09401*.

[13] F. Guidi and D. Dardari, "Radio positioning with EM processing of the spherical wavefront," *IEEE Trans. Wireless Commun.*, vol. 20, no. 6, pp. 3571–3586, Jun. 2021.

[14] K. Keykhosravi, M. F. Keskin, G. Seco-Granados, and H. Wymeersch, "SISO RIS-enabled joint 3D downlink localization and synchronization," in *Proc. IEEE Int. Conf. Commun.*, Jun. 2021, pp. 1–6.

[15] M. Rahal, B. Denis, K. Keykhosravi, B. Uguen, and H. Wymeersch, "RIS-enabled localization continuity under near-field conditions," in *Proc. IEEE 22nd Int. Workshop Signal Process. Adv. Wireless Commun. (SPAWC)*, Sep. 2021, pp. 436–440.

[16] J. He, H. Wymeersch, L. Kong, O. Silvén, and M. Juntti, "Large intelligent surface for positioning in millimeter wave MIMO systems," in *Proc. IEEE 91st Veh. Technol. Conf.*, Jun. 2020, pp. 1–5.

[17] R. Ghazalian, K. Keykhosravi, H. Chen, H. Wymeersch, and R. Jäntti, "Bi-static sensing for near-field RIS localization," in *Proc. IEEE Global Commun. Conf.*, Dec. 2022, pp. 6457–6462.

[18] M. Meles, A. Rajasekaran, L. Mela, R. Ghazalian, K. Ruttik, and R. Jäntti, "Performance evaluation of measurement based GPS denied 3D drone localization and tracking," in *Proc. IEEE Wireless Commun. Netw. Conf. (WCNC)*, Mar. 2023, pp. 1–6.

[19] M. Ammous and S. Valaee, "Cooperative positioning with the aid of reconfigurable intelligent surfaces and device-to-device communications in mmWave," in *Proc. IEEE 33rd Annu. Int. Symp. Pers., Indoor Mobile Radio Commun. (PIMRC)*, Sep. 2022, pp. 683–688.

[20] A. Fascista, A. Coluccia, H. Wymeersch, and G. Seco-Granados, "RIS-aided joint localization and synchronization with a single-antenna mmWave receiver," in *Proc. IEEE Int. Conf. Acoust., Speech Signal Process. (ICASSP)*, Jun. 2021, pp. 4455–4459.

[21] P. Gertzell, J. Landelius, H. Nyqvist, A. Fascista, A. Coluccia, G. Seco-Granados, N. Garcia, and H. Wymeersch, "5G multi-BS positioning with a single-antenna receiver," in *Proc. IEEE 31st Annu. Int. Symp. Pers., Indoor Mobile Radio Commun.*, Aug. 2020, pp. 1–5.

[22] W. Chen, S. He, Q. Xu, J. Ren, Y. Huang, and L. Yang, "Positioning algorithm and AoD estimation for mmWave FD-MISO system," in *Proc. 10th Int. Conf. Wireless Commun. Signal Process. (WCSP)*, Oct. 2018, pp. 1–6.

[23] H. Guo, Y.-C. Liang, J. Chen, and E. G. Larsson, "Weighted sum-rate maximization for reconfigurable intelligent surface aided wireless networks," *IEEE Trans. Wireless Commun.*, vol. 19, no. 5, pp. 3064–3076, May 2020.

[24] A. Fascista, M. F. Keskin, A. Coluccia, H. Wymeersch, and G. Seco-Granados, "RIS-aided joint localization and synchronization with a single-antenna receiver: Beamforming design and low-complexity estimation," *IEEE J. Sel. Topics Signal Process.*, vol. 16, no. 5, pp. 1141–1156, Aug. 2022.

[25] J. An, C. Xu, L. Gan, and L. Hanzo, "Low-complexity channel estimation and passive beamforming for RIS-assisted MIMO systems relying on discrete phase shifts," *IEEE Trans. Commun.*, vol. 70, no. 2, pp. 1245–1260, Feb. 2022.

[26] J.-S. Jung, C.-Y. Park, J.-H. Oh, and H.-K. Song, "Intelligent reflecting surface for spectral efficiency maximization in the multi-user MISO communication systems," *IEEE Access*, vol. 9, pp. 134695–134702, 2021.

[27] J. He, H. Wymeersch, T. Sanguanpuak, O. Silven, and M. Juntti, "Adaptive beamforming design for mmWave RIS-aided joint localization and communication," in *Proc. IEEE Wireless Commun. Netw. Conf. Workshops (WCNCW)*, Apr. 2020, pp. 1–6.

[28] Z. Abdullah, A. Papazafeiropoulos, S. Kisseleff, S. Chatzinotas, and B. Ottersten, "Impact of phase-noise and spatial correlation on double-RIS-assisted multiuser MISO networks," *IEEE Wireless Commun. Lett.*, vol. 11, no. 7, pp. 1473–1477, Jul. 2022.

[29] L. Cheng, Q. Zhu, C.-X. Wang, W. Zhong, B. Hua, and S. Jiang, "Modeling and simulation for UAV air-to-ground mmWave channels," in *Proc. 14th Eur. Conf. Antennas Propag. (EuCAP)*, Mar. 2020, pp. 1–5.

[30] P. Wang, J. Fang, H. Duan, and H. Li, "Compressed channel estimation for intelligent reflecting surface-assisted millimeter wave systems," *IEEE Signal Process. Lett.*, vol. 27, pp. 905–909, 2020.

[31] X. Wei, D. Shen, and L. Dai, "Channel estimation for RIS assisted wireless communications—Part I: Fundamentals, solutions, and future opportunities," *IEEE Commun. Lett.*, vol. 25, no. 5, pp. 1398–1402, May 2021.

[32] O. E. Ayach, S. Rajagopal, S. Abu-Surra, Z. Pi, and R. W. Heath, "Spatially sparse precoding in millimeter wave MIMO systems," *IEEE Trans. Wireless Commun.*, vol. 13, no. 3, pp. 1499–1513, Mar. 2014.

[33] Y. Tsai, L. Zheng, and X. Wang, "Millimeter-wave beamformed full-dimensional MIMO channel estimation based on atomic norm minimization," *IEEE Trans. Commun.*, vol. 66, no. 12, pp. 6150–6163, Dec. 2018.

[34] T. Ma, Y. Xiao, X. Lei, L. Zhang, Y. Niu, and G. K. Karagiannidis, ''Reconfigurable intelligent surface assisted localization: Technologies, challenges, and the road ahead,'' *IEEE Open J. Commun. Soc.*, vol. 4, pp. 1430–1451, 2023.
[35] J. He, H. Wymeersch, and M. Juntti, ''Leveraging location information for RIS-aided mmWave MIMO communications,'' *IEEE Wireless Commun. Lett.*, vol. 10, no. 7, pp. 1380–1384, Jul. 2021.
[36] C. Singh, K. Singh, and K. H. Liu, ''Fast beam training for RIS-assisted uplink communication,'' 2021, *arXiv:2107.14138*.
[37] D. Simon, ''Kalman filtering,'' *Embedded Syst. Program.*, vol. 14, no. 6, pp. 72–79, Jun. 2001.
[38] V. Madyastha, V. Ravindra, S. Mallikarjunan, and A. Goyal, ''Extended Kalman filter vs. Error state Kalman filter for aircraft attitude estimation,'' in *Proc. AIAA Guid., Navigat., Control Conf.*, Aug. 2011, p. 6615.
[39] M. Meles, L. Mela, A. Rajasekaran, K. Ruttik, and R. Jäntti, ''Drone localization based on 3D-AoA signal measurements,'' in *Proc. IEEE 95th Veh. Technol. Conf.*, Jun. 2022, pp. 1–5.
[40] D. Jeon, H. Choi, and J. Kim, ''UKF data fusion of odometry and magnetic sensor for a precise indoor localization system of an autonomous vehicle,'' in *Proc. 13th Int. Conf. Ubiquitous Robots Ambient Intell. (URAI)*, Aug. 2016, pp. 47–52.
[41] S. Julier, J. Uhlmann, and H. F. Durrant-Whyte, ''A new method for the nonlinear transformation of means and covariances in filters and estimators,'' *IEEE Trans. Autom. Control*, vol. 45, no. 3, pp. 477–482, Mar. 2000.
[42] K. P. B. Chandra, D.-W. Gu, and I. Postlethwaite, ''Square root cubature information filter,'' *IEEE Sensors J.*, vol. 13, no. 2, pp. 750–758, Feb. 2013.
[43] P. Stoica, E. G. Larsson, and A. B. Gershman, ''The stochastic CRB for array processing: A textbook derivation,'' *IEEE Signal Process. Lett.*, vol. 8, no. 5, pp. 148–150, May 2001.
[44] P. Stoica and A. Nehorai, ''MUSIC, maximum likelihood, and cramer-rao bound,'' *IEEE Trans. Acoust., Speech, Signal Process.*, vol. 37, no. 5, pp. 720–741, May 1989.
[45] T. Li and A. Nehorai, ''Maximum likelihood Direction-of-Arrival estimation of underwater acoustic signals containing sinusoidal and random components,'' *IEEE Trans. Signal Process.*, vol. 59, no. 11, pp. 5302–5314, Nov. 2011.
[46] Z. Abu-Shaban, K. Keykhosravi, M. F. Keskin, G. C. Alexandropoulos, G. Seco-Granados, and H. Wymeersch, ''Near-field localization with a reconfigurable intelligent surface acting as lens,'' in *Proc. IEEE Int. Conf. Commun.*, Jun. 2021, pp. 1–6.
[47] L. Han, R. Liu, Z. Wang, X. Yue, and J. S. Thompson, ''Millimeter-wave MIMO-NOMA-based positioning system for Internet-of-Things applications,'' *IEEE Internet Things J.*, vol. 7, no. 11, pp. 11068–11077, Nov. 2020.
[48] F. Ghaseminajm, M. Alsmadi, D. Tubail, and S. S. Ikki, ''RIS-aided mobile localization error bounds under hardware impairments,'' *IEEE Trans. Commun.*, vol. 70, no. 12, pp. 8331–8341, Dec. 2022.


**MEHARI MELES** (Member, IEEE) received the B.Sc. degree in electronics and communication engineering from the Mekelle Institute of Technology (MIT), Ethiopia, in 2008, the master's degree in communication and radar systems from the School of Electrical and Computer Engineering, Defence University, Ethiopia, in 2014, and the advanced master's degree in space applications and services from ISAE-SUPAERO, France, in 2018. He is currently pursuing the Ph.D. degree with the Department of Information and Communication Engineering, Aalto University.

In parallel to his academic achievements, he was a Researcher with the Information National Security Agency (INSA), Ethiopia, focusing on communications and signal processing, from 2009 to 2012, from 2015 to 2016, and from 2019 to 2020. His research interests include global navigation satellite system (GNSS) free localization, tracking, and antenna array signal processing.

**AKASH RAJASEKARAN** received the B.Tech. degree in aerospace engineering from the Amrita School of Engineering, India, and the M.Sc. degree in aerodynamics from Cranfield University, U.K. He is currently pursuing the Ph.D. degree with Aalto University, under the supervision of Prof. Riku Jäntti. His doctoral work explores global navigation satellite system (GNSS) free autonomous navigation of unmanned aerial vehicles.

**LAURI MELA** received the B.Sc. degree in communications engineering and the M.Sc. degree in acoustics and audio technology from the School of Electrical Engineering, Aalto University, Finland, in 2013 and 2023, respectively, where he is currently pursuing the Ph.D. degree with the Department of Information and Communications Engineering. His current research interests include visible light communications (VLC) enabled radio frequency backscatter devices and reconfigurable intelligent surfaces.

**RIKU JÄNTTI** (Senior Member, IEEE) received the M.Sc. degree (Hons.) in electrical engineering and the D.Sc. degree (Hons.) in automation and systems technology from the Helsinki University of Technology (TKK), in 1997 and 2001, respectively. He is currently a Full Professor with the Department of Information and Communications Engineering, School of Electrical Engineering, Aalto University, Finland. Prior to joining Aalto University, in August 2006, he was a Professor (pro tem) with the Department of Computer Science, University of Vaasa. His research interests include machine type communications, disaggregated radio access networks, backscatter communications, quantum communications, and radio frequency inference. He is a member of the editorial board of the IEEE Transactions on Cognitive Communications and Networking. He has been an IEEE VTS Distinguished Lecturer (Class 2016).